January 1977

ON THE GROWTH OF STEAM DROPLETS FORMED IN A LAVAL NOZZLE USING BOTH STATIC PRESSURE AND LIGHT SCATTERING MEASUREMENTS

by

Clifford A. Moses and Gilbert D. Stein

Report #2 prepared for Contract N00014-76-C-0378: "Investigation of Metal and Metal Oxide Clusters Small Enough to Constitute the Critical Size for Gas Phase Nucleation in Combustion Processes" (Power Branch, Office of Naval Research, Arlington, VA.). Submitted by Gilbert D. Stein, Principal Investigator.

NORTHWESTERN UNIVERSITY

Department of Mechanical Engineering
And Astronautical Sciences

Evanston, Illinois 60201

SECURITY CLASSIFICATION OF THIS PAGE (When Data Entered)

REPORT DOCUMENTATION PAGE

READ INSTRUCTIONS BEFORE COMPLETING FORM

1. REPORT NUMBER: N00014-76-C-0378-TR1
2. GOVT ACCESSION NO.
3. RECIPIENT'S CATALOG NUMBER

4. TITLE (and Subtitle): ON THE GROWTH OF STEAM DROPLETS FORMED IN A LAVAL NOZZLE USING BOTH STATIC PRESSURE AND LIGHT SCATTERING MEASUREMENTS.
5. TYPE OF REPORT & PERIOD COVERED: Technical Report.
6. PERFORMING ORG. REPORT NUMBER

7. AUTHOR(s): Clifford A. Moses and Gilbert D. Stein
8. CONTRACT OR GRANT NUMBER(s): N00014-76-C-0378

9. PERFORMING ORGANIZATION NAME AND ADDRESS: Northwestern University, Dept. of Mechanical Engineering and Astronautical Sciences - Evanston, IL 60201
10. PROGRAM ELEMENT, PROJECT, TASK AREA & WORK UNIT NUMBERS: NR092-544

11. CONTROLLING OFFICE NAME AND ADDRESS: Office of Naval Research, Arlington, VA 22217
12. REPORT DATE: January 1977
13. NUMBER OF PAGES: 43

14. MONITORING AGENCY NAME & ADDRESS (if different from Controlling Office): ONR, Chicago, 536 South Clark Street, Chicago, IL 60605 — 47 p.
15. SECURITY CLASS. (of this report): Unclassified
15a. DECLASSIFICATION/DOWNGRADING SCHEDULE

16. DISTRIBUTION STATEMENT (of this Report): Distribution of this document is unlimited. — 14 TR-1

17. DISTRIBUTION STATEMENT (of the abstract entered in Block 20, if different from Report)

18. SUPPLEMENTARY NOTES

19. KEY WORDS (Continue on reverse side if necessary and identify by block number): Light Scattering, Nucleation, Droplet Growth, Steam Clusters, Supersonic Flow, Laval Nozzle.

20. ABSTRACT (Continue on reverse side if necessary and identify by block number)

A series of experiments on steam condensation have been made in a Laval nozzle over a variety of starting conditions such that the onset of condensation occurs in the range -40 to 40°C. The homogeneous nucleation and growth of the new phase is documented with both static pressure and laser light scattering. Since even at onset the majority of the condensed phase is due to droplet growth the nucleation and growth are coupled and the availability of two measured quantities is helpful in comparing a →

DD FORM 1 JAN 73 1473 EDITION OF 1 NOV 65 IS OBSOLETE
S/N 0102-014-6601 | i.

SECURITY CLASSIFICATION OF THIS PAGE (When Data Entered)

403 562

1B

particular combination of nucleation rate and growth law. For detailed calculations on one of the experiments there is excellent agreement with both measurements throughout the condensation zone and a theoretical calculation using the classical nucleation rate expression due to Volmer and a droplet growth law due to Gyarmathy.

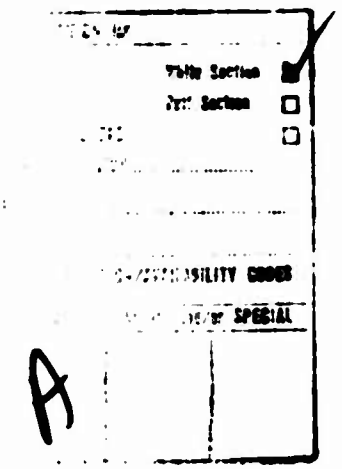

NOMENCLATURE

A	nozzle flow area
A^*	nozzle flow area at throat
C	correction factor to nucleation rate
c_o	concentration of vapor molecules at time zero
c	agglomeration sticking coefficient
g	mass fraction of flow that has condensed
ΔG^*	change in Gibb's free energy in the formation of a critical-sized cluster
h	enthalpy, height of slit used to define the solid angle of the scattered beam in light-scattering experiments
I, I_θ	intensity of scattered light, in particular at $\theta = 90^o$
I_o	intensity of incident laser beam
J	nucleation rate, number of critical clusters formed/cm^3/sec
k	Boltzmann's constant 1.38×10^{-16} ergs/mole, wave number
ℓ	length of detector window
L	latent heat of vaporization
$\dot{m}$; m_v, m_c	mass flow rate of steam in the nozzle; subscripts sometimes used to distinguish between the vapor phase and the condensate
m	mass of one molecule, index of refraction
n	number of clusters per unit mass of vapor
N	concentration of clusters in the flow
N_o	concentration of clusters in the flow at time zero
dN_i^t	the number of clusters nucleated in the nozzle in the range x_i and $x_i + dx$ in a time $dt = dx/u_i$

p, p_v	local pressure of the vapor
$p_\infty(T)$	liquid/vapor equilibrium pressure at temperature T
p_o	pressure in stagnation chamber of nozzle
P_l	laser power - watts
q	heat released during condensation
$\bar{r}$	mean droplet radius
r	droplet radius
r^*	critical radius for cluster formation
r_{ij}	radius of a droplet born at position i and grows to position j
R	gas constant, distance from light scattering volume to detector
S	supersaturation ratio, p_v / p_∞
t	time
T	local temperature of vapor
T_o	temperature in stagnation chamber of nozzle
u	flow velocity
v_c	volume per molecule in the condensed phase
V	scattering volume
x	position in nozzle

Greek letters

α	thermal accommodation coefficient used in Hill's growth model, polarizability
β	molecular impingement rate used in Hill's growth model
λ_{th}	thermal conductivity
λ_c	mean free path for molecular collisions
λ	light-scattering: wavelength of laser beam

μ	molecular weight
ξ	mass accommodation coefficient
ρ	density of vapor
ρ_c	density of condensate
$\sigma, \sigma_\infty(T)$	surface tension, subscript ∞ refers to bulk value for a flat surface ($r = \infty$) and is a function only of temperature
$d\sigma/d\Omega$	differential scattering cross-section per unit solid angle - cm^2 steradian^{-1}
$(d\sigma/d\Omega)_V$	differential scattering cross-section per unit solid angle per unit volume in the flow - cm^{-1} steradian^{-1}
$(d\sigma/d\Omega)_{SV}$	differential scattering cross-section per unit solid angle from the scattering volume - cm^2 steradian^{-1}
θ	scattering angle

INTRODUCTION

The primary purpose of this communication is to examine the growth of steam droplets formed via homogeneous nucleation in a supersonic Laval nozzle using both static pressure and light scattering measurements taken through the nucleation and growth region along the flow direction. The goal is to make some relative assesment of the merits of the particular growth laws investigated and to examine the effect of these growth laws on the predicted condensation onset for a given version of the nucleation rate equation. It will be seen that in steam condensation the nucleation and growth processes are coupled in that a variation of either will cause a shift in the predicted point of onset. This is not the case in condensation in a carrier gas, such as moist air expansions, in which the nucleation is over before any appreciable amount of growth has occurred (e.g. the condensate mass fraction at onset is typically 0.001 in the former case and 0.0001 in the latter).

The use of supersonic Laval nozzles for steam turbines and rocket engines has a long and much published history. The study of condensation phenomena in nozzles also has a rich history including Stodola [1] in the 1920's, Binnie and co-workers [2,3] the 1930's, Oswatitsch [4-6] in the 1940's, increased activity in this field in the 1950's [7-12], Gyarmathy [13,14] and Hill [15-17] in the 1960's and Barschdorf [18-21] in the 1970's, with perhaps the most ardent proponent over the past twenty years for the nozzle as a means of studying condensation being Wegener and co-workers [22-30]. The nucleation aspects of the steam condensation work presented here have been published earlier [31]. The advantages of the nozzle for study of the homogeneous nucleation process has been extolled many times over in the above references and will thus not be repeated here. The merits of laser light scattering in the detection of condensation and the measurement of cluster concentration and size have also been enumerated [26,31-33].

DESCRIPTION OF THE PROCESS

The nozzle is designed so that the flow can be treated as a steady, one dimensional, inviscid, attached supersonic expansion. The process is illustrated in Fig. 1. The steam expands isentropically from the stagnation chamber at point 1 into the converging portion of the nozzle. It crosses the vapor-liquid equilibrium line at 2 where the saturation ratio $S = (p/p_\infty)_T = 1$, i.e. the steam is saturated vapor. Depending on the initial conditions p_o and T_o, point 2 may occur in the converging (subsonic) part of the nozzle or in the diverging (supersonic) section. Since the expansion cools the gas at about 10^6 $^oC/sec$, phase change does not occur at 2 but continues down the isentrope becoming supersaturated until sufficient nuclei of the new phase form to cause a perceptable rate of change to the new state at point 3, the onset of condensation. This point is commonly defined as that at which the pressure differs from the isentrope by 1%. It is at this point that the light scattering is first seen [34]. In steam nozzles, the saturation ratio at this point typically ranges from $S \simeq 4$ to 15, depending on the initial conditions. The diameter of the nuclei are of the order of 10^{-7} cm. As the flow continues, the vapor condenses onto these nuclei; the heat that is released forces the thermodynamic properties away from the isentrope to point 4. The length along the nozzle between points 3 and 4 is known as the "condensation zone". At the end of the condensation zone, the thermodynamic state of the vapor is near the equilibrium line. The processes for droplet growth slow down and the flow again begins to expand and cool.

By varying the starting pressure and temperature p_o and T_o (point 1 in Fig. 1A and 1C) the steam can be expanded along different isentropes such that the nucleation process, which occurs near point 3, can be examined through the triple point temperature. This region is accessible mainly by varying p_o from 600 to 60 torr. The temperature T_o is in the range of 90-110°C.

The governing equations for the nozzle flow are:

continuity,

$$\frac{d\rho}{\rho} + \frac{dA}{A} + \frac{du}{u} = \frac{dg}{1-g} \tag{1}$$

or

$$\rho A u = \dot{m} \quad ,$$

momentum,

$$\rho u du + dp = 0 \quad , \tag{2}$$

energy,

$$d\left(h + \frac{u^2}{2}\right) = dq \cong Ldg \quad , \tag{3}$$

and state,

$$p = (1-g)\rho RT/\mu \quad , \tag{4}$$

The effective area ratio A is obtained by running the nozzle at the inlet pressure of interest and a high enough temperature so there is no condensation in the nozzle. Thus we have 4 equations (1)-(4) and 5 unknowns ρ, p, T, u and g. One way to close the system is to measure one property such as pressure, i.e. Fig. 1A. Then p and T as shown in Fig. 1C, g as shown in 1B and ρ and u can each be determined at every point in the nozzle. The approximately equal sign of $dq \cong Ldg$ is due to the fact that the droplet temperature will always be higher than the local vapor temperature, thus $Ldg > dq$. The other way to close the system of Eqs. (1)-(4) is to use a nucleation rate equation and droplet growth law which can be used to express g as a function of the remaining unknowns above. The rate

equation for homogeneous nucleation used here is the classical expression due to Volmer [35, 36] which treats the embryonic cluster of the new phase as a macroscopic, motionless, spherical liquid droplet,

$$J = C\left(\frac{p}{kT}\right)^2 \left(\frac{2\sigma}{\pi m}\right)^{1/2} v_c \exp(-\Delta G^*/kT) \quad , \tag{5}$$

where J is the number of critical size clusters formed per sec per cm^3, and ΔG^* the Gibbs free energy of formation of the critical sized cluster $\Delta G^* = \frac{4}{3}\pi r^{*2}\sigma$. The critical radius is given by the Gibbs-Thompson-Helmholtz equation

$$r^* = 2\sigma\, v_c/kT\, \ell n\, (p/p_\infty) \quad . \tag{6}$$

Since the cluster size is much smaller than the vapor mean free path (i.e. Knudsen number $\gg$ 1) the growth law is simplified, one version of which is due to Hill [15],

$$dr/dt = \xi(p-p_D)v_c/(2\pi\, mkT)^{1/2} \quad , \tag{7}$$

where $p_D = p_\infty \exp(2\sigma\, v_c/kTr)$ from Eq. (6). It is the matter of the growth law that is primarily being considered in this work so various prescriptions will be examined later in the paper.

Thus the use of the full set of equations (1)-(7) will be closed and all the thermodynamic data as well as a detailed cluster size distribution and concentration can be calculated for every location in the nozzle. All of the properties plotted in Fig. 1 can be obtained theoretically.

It is near the point of onset that the light scattering is first seen, Fig. 1D. In this experiment molecular scattering upstream of the onset of condensation cannot be detected above the photomultiplier dark current.

Since Eq. (6) predicts an approximate starting size of $r^* \tilde{=} 5\text{Å}$ the light scattering for one cluster will follow the Rayleigh scattering law for plane polarized light with its electric field perpendicular to the plane of observation,

$$d\sigma/d\Omega = \alpha^2 k^4 \quad , \tag{8}$$

where α is the polarizability $\alpha = (m^2 - 1/m^2 + 2)r^3$ and k the wave number $k = 2\pi/\lambda$.

For independent scattering from a unit volume of the flow containing N clusters with a normalized size distribution f(r), the cross section is

$$(d\sigma/d\Omega)_V = N \left(\frac{m^2 - 1}{m^2 + 2}\right)^2 \left(\frac{2\pi}{\lambda}\right)^4 \int_o^\infty r^6 f(r)dr \quad , \tag{9}$$

and is related to the measured light intensities and scattering geometry by

$$(d\sigma/d\Omega)_V = (d\sigma/d\Omega)_{SV}/V \quad ,$$

$$= \frac{I_\theta R^2/h\ell^2}{I_o} \quad , \tag{10}$$

where $(d\sigma/d\Omega)_{SV}$ is the differential scattering cross section for the scattering volume V defined by the laser beam cross section and the detector window length ℓ. The mass condensed per unit volume in the flow is

$$g\rho = (N4\pi/3v_c) \int r^3 f(r)dr \quad . \tag{11}$$

If the distribution function f(r) is known then comparison to experiment can be made using the gasdynamic measurements and Eq. (11) or the light scattering measurements and Eq. (10). If a distribution function with an additional variable is used, say mean radius $\bar{r}$, then Eqs. (10) and (11) can be used to obtain $\bar{r}$ and N. Using Eq. (5) the number of clusters born at x_i is

$$dN_i^t = J(x_i)A(x_i)dx\, dt = J(x_i)A(x_i)dx_i \frac{dx}{u_i} \quad , \tag{12}$$

and their size at any later position, j, is

$$r_{ij}(x_j) = \int_{x_i}^{x_j} \frac{dr}{dt} \frac{1}{u} dx \quad . \tag{13}$$

The mass condensed in any increment of the nozzle is the sum of the mass of the new clusters born in the increment via the nucleation rate plus the growth of all droplets born upstream of the increment:

$$dm_{cj} = \frac{4}{3}\pi r_j^3 \rho_c dN_j^t + \sum_{i=1}^{j} 4\pi r_{ij}^2 \rho_c \left(\frac{dr}{dt}\right)_{r_{ij}} \frac{u_i}{u_j} dN_i^t \qquad (14)$$

where dN_j^t and r_{ij} are given above in Eqs. (12) and (13).

EXPERIMENTAL

The nozzle is two dimensional, made of black anodized aluminum with a throat 1 cm x 1 cm, and has a window on one sidewall. A schematic arrangement is shown in Figure 2. Steam enters from the side through the stagnation chamber, into the nozzle, through a glass tee to a condenser and finally to a vacuum pump. There are ports at either end to accommodate static pressure probes or window and light trap for the laser. Static pressure on the nozzle centerline is taken with a stainless steel tube of 0.75 mm diameter, sealed at one end, a pressure transducer at the other, and a 0.25 mm hole in the side of the tube where the pressure is to be measured. The ports have ball valves installed so that the pressure probe can be removed without disturbing the flow and a window and light trap installed for the light scattering. The flow is traversed by the probe or light scattering photomultiplier by moving the stagnation chamber-nozzle-glass tee assembly. Thus the laser and photomultiplier arrangement can be aligned once and then remain stationary. The light source used is a continuous wave, 4 watt argon ion laser with a intracavity prism for tuning. With almost 2 watts of power at the 514.5 nm line small slits for good resolution and an ordinary uncooled photomultiplier (RCA 1P21) can be used. The slits are 0.6 mm in the flow direction by 3 mm vertically, to ensure cutting off the complete laser beam forming the scattering volume.

The experimental procedure then is to install the pressure probe, turn on the steam flow, take pressure data after steady conditions prevail, remove the probe, install window and light trap, and take light scattering data. Due to the time lag in the probe, pressure data is taken at discrete points in the nozzle waiting for pressure equilibration at each point. The pressure data is taken in 10-30 minutes depending on the inlet (stagnation) pressure p_o. The light scattering data is taken in about 10 seconds.

The steam for this work was tapped off a convenient line of the University's steam heating system. The flow was filtered through a sintered, stainless steel filter of 0.4 micron rating. The line pressure was reduced from 40 psig to atmospheric where it was regulated by a large plastic bag. A second valve reduced the pressure to the desired stagnation pressure. A by-pass line around the nozzle was provided to dry out the lines before an experiment was conducted. The valves and piping between the filter and the stagnation chamber were either brass or stainless steel to prevent corrosion and flaking into the steam flow. Also, these valves and lines had to be heated by thermal tapes to prevent the steam from condensing prior to the test section. Unfortunately, this limited the minimum stagnation temperatures to about 95 ^{o}C and prevented thorough investigations at stagnation pressures below around 160 torr as the expansion required to sufficiently cool the flow for nucleation was too great.

The nozzle exit was connected to a Kinney vacuum pump, rated at 485 cfm flow rate. Care had to be taken to condense out most of the steam before it got to the pump to prevent it condensing in the pump and emulsifying the oil. A shell and tube heat exchanger was used to cool the steam. A condensate trap removed the resulting water from the flow. The system was able to remove about 95% of the steam as condensate.

The actual geometry of the nozzle was chosen for ease of fabrication with the additional criterion of curve continuity through the second derivative. The expansion was in one dimension with a glass window for one of the flat surfaces. The profile of the transonic and supersonic sections was a circular arc of 68.6 cm radius; this was mated smoothly with an arc of 5.3 cm radius to form the subsonic entrance. The choice of a circular arc is to allow the profile to be machined on a numerically-controlled milling machine with circular interpolation, i.e., one that mills a constant radius arc between two points rather than a straight line. The actual profile is presented as part of Fig. 3 and

compared with the "effective profile", the difference being the result of the displacement thickness of the boundary layer.

Except for the window, the nozzle was machined from aluminum. Each piece was then "vapor blasted" and black anodized to provide flat-black surfaces to reduce the reflections. ("Vapor blasting" is similar to sand blasting only much finer. The process does not appreciably change the dimensions.)

Effect of Laser Power

Theoretically, very little light should be absorbed by the water due to its low absorption cross section. Thus the presence of the laser beam should not affect the nucleation process. As an experimental test the scattered light was recorded through the nucleation and growth zone for several experiments with constant flow conditions but with laser power varied from 0.1 to 1.5 watts, a factor of 15:1. The results shown in Fig. 4 confirms that the laser, at least in the power range used here, does not affect the phase change. There is evidence from diffusion cloud chamber research, that some wave lengths in the ultraviolet will enhance water nucleation [37].

Heterogeneous Nucleation Tests

Heterogeneous nucleation is not usually considered an effective mechanism in nozzle flows because of the extremely short time scales involved [23]. However, because the steam supply for this work came from the University's heat and power plant, the purity could not be controlled except by filtration. A sample of condensed steam was analyzed for impurities and a level of about 1 ppm total solids was found to be present in the form of iron, and silicate and carbonate salts presumably from the piping and carry-over from the boiler water. The experiments involved placing different degrees of filtration in the steam supply line as listed below:

1. 0.4 micron filter
2. 0.4 and 0.008 micron filters
3. 0.4, 0.008 micron filters and an activated charcoal bed
4. 0.4, 0.008 micron filters and two activated charcoal beds

Representative onsets are presented in Fig. 5. There are no significant differences in the onsets for all four stages of increased filtering. Also the static pressure traces showed no unusual shapes in any of these experiments.

Comparison of Pressure and Light Scattering Onsets

The onset criteria used here is a 1% pressure increase over the isentropic value, and a light scattering signal rising out of the phototube background, a value of $I/I_o \cong 10^{-14}$. The data plotted in Fig. 6 shows that the two criteria are quite equivalent.

Under some circumstances it is difficult and time consuming to make pressure measurements in an effort to find the phase change onset such as experiments at low pressure or experiments with condensates having small latent heats of vaporization. Light-scattering measurements, on the other hand, are relatively easy to obtain and can be used to determine the location of the onset. The least ambiguous circumstances for determining the onset with light scattering is that in which the laser is so powerful and/or the detector so sensitive that the molecular Rayleigh scattering can be seen upstream of the condensation zone. This has been accomplished using a pulsed ruby laser in a free jet expansion [38]. In addition, up to the point of significant clustering the light scattering can be used as a density measurement with proper scattering system calibration and knowing the molecular scattering cross section.

Measurements Through the Condensation Zone

A systematic series of experiments were conducted in which the effect of initial temperature and pressure variation on the condensation zone was documented. Some of the static pressure histories are shown in Fig. 7 for pressure held constant at approximately 300 Torr in 7A and 400 Torr in 7B. With temperature held constant $T_o = 100^oC$ the effect of p_o variation is shown in Fig. 7C. The expected qualitative results are evident in which there is a delayed onset with increasing temperature, holding p_o constant, and with decreasing pressure, holding T_o constant. The above trends shift the starting point of the expansion away from the vapor-liquid equilibrium on a p-T diagram, and thus the onset occurs at higher Mach number which is of course further down the nozzle.

The earlier onsets have a steeper rise in pressure and a greater Δp above the isentrope. The difference in pressure rise in Fig. 6 is about a factor of 2 or less from highest to lowest.

The variation in light scattering with p_o is seen in Fig. 8 with the same qualitative variation as in Fig. 7A and B. The shapes of curves are all about the same with a factor of 4 or less variation in signal downstream of the onsets, i.e. point 4 in Fig. 1. Thus the light scattering is more sensitive to changes in the onset and growth conditions than the heat release measurement inferred from static pressure measurement. This is a manifestation of different dependencies on the droplet size distribution, the mass condensed being proportional to third moment (i.e. $\int r^3 f(r)dr$, Eq. (11)) while the light scattering is proportional to the sixth moment, Eq. (9). Thus the light scattering is more sensitive to changes in the size distribution than the static pressure measurement.

GROWTH LAWS

Once the critical-sized clusters have formed, they are carried with the flow and provide surfaces onto which the supercooled vapor can condense. Two mechanisms are involved in the growth of a droplet from the vapor phase: the transfer of mass between the vapor and the droplet and the transfer of heat from the droplet to the vapor as the latent heat is released by the "condensing" molecules. The theory for the growth is simplified if the Knudsen number $K_n = \lambda_c / r \gg 1$, i.e. the collision mean free path is much greater than the droplet radius. In this work, the mean free path in the condensation zone is of the order of 10^{-5} cm whereas the largest droplets will be of the order of 10^{-6} cm so it is anticipated that droplet growth for this work can be best described by the concepts of free molecular flow.

Two approaches to the growth theory are considered here. One is to approach the problem from the viewpoint of kinetic theory while the other is to use macroscopic concepts of heat and mass transfer and apply correction factors based on the Knudsen number. Two growth laws, based on the above approaches, have been published respectively by Hill [15] and Gyarmathy [39].

Hill [15] developed a growth law from the viewpoint of kinetic theory by considering the growth rate of the droplet to be the difference between the molecular impingement rate of the vapor at the droplet surface and the evaporation rate of the droplet,

$$\frac{dr}{dt} = \frac{\xi}{\rho_c}\left[\frac{p}{\sqrt{2\pi\, RT}} - \frac{p_D}{\sqrt{2\pi\, RT_D}}\right] = \frac{\xi}{\rho_c}\left[\beta_{con.} - \beta_{evap.}\right] \quad . \tag{15}$$

p_D is the (hypothetical) ambient pressure which would keep the droplet in equilibrium with a surrounding vapor at a temperature equal to that of the droplet, T_D. In this state, the evaporation rate would just balance the impingement rate. From Eq. (6) for the equilibrium droplet size, $p_D = p_\infty(T_D)\, \exp\{2\sigma/(\rho_c R T_D r)\}$. The mass

accommodation coefficient is ξ, i.e., that fraction of the impinging vapor molecules that actually penetrate the surface. The remainder are reflected after achieving some degree of thermal equilibrium designated by a thermal accommodation coefficient α. These coefficients are used to average out detailed surface interactions. Their values are open to question but are usually taken as $\alpha = 1.0$ and $.04 < \xi < 1.0$ (e.g. [15], [40-44]). Hill determined the droplet temperature from a balance of the net energy flux to the droplet with the increase in internal energy.

Gyarmathy [39] combines Fick's law of diffusion and Fourier's law of heat conduction to develop a rate of growth for a spherical droplet in a continuum environment of arbitrary supersaturation and moisture fraction. To extend the validity of the expression to cases of smaller droplets, a correction factor is invoked which is a function of the Knudsen number. For the case of pure steam, his growth rate reduces to the following expression

$$\frac{dr}{dt} = \frac{1 - \frac{r^*}{r}}{r + 1.59\lambda_c}\left[\frac{\lambda_{th} RT^2}{L^2}\right] \ell n\ S. \qquad (16)$$

Both treatments however contain an element of uncertainty. Gyarmathy's involves an adjustment for free-molecular flows, while Hill uses the mass and thermal accommodation coefficients. Since both growth rates are functions of droplet radius, at each point in the nozzle they must be evaluated for each species of droplet size. Hill's method is time consuming as it involves the solution of two simultaneous, non-linear equations for each case. To reduce this effort, Hill evaluated the growth rate for a surface-averaged size droplet at each step and applied this growth to all droplet sizes. If this prescription is followed an additional uncertainty is introduced.

In Fig. 9 these growth rates are compared as functions of droplet size for conditions typical of onset in this work, T = 280°K and p = 68 torr, corresponding to a saturation ratio of S = 9.5. The surface-averaged growth rate is shown dashed at a typical value for ζ = 1 and 0.04 because its magnitude depends on the exact distribution of droplet sizes. Note the large growth rate applied to newly formed clusters as compared to the radius-dependent models. The growth law due to Wu [45] is constant at small radii but matches to a radius-dependence growth model at larger r. However for the conditions of these experiments the constant growth is always larger than the radius-dependent part and thus operates here as a purely constant growth law.

As an illustration of the effect of the growth laws on the detailed evolution of the phase change, three growth models were applied to the theoretical description using the equations for the gasdynamics and nucleation. The example is shown in Fig. 10 for the initial conditions of Experiment 252 and is used here to show the relative effects of the three growth laws. Note that an unrealistically high value of mass accommodation (ζ = 1 is an upper limit) has been employed in this particular set of calculations. One difference between the average-radius model and the radius-dependent models is the fate of clusters "born" after onset. As the thermodynamic state of the flow shifts back toward the liquid-vapor equilibrium line, r^* increases. Under the radius-dependent growth models, those clusters born after onset begin with zero growth rate and as r^* increases they are therefore constrained to evaporate. The average-growth model allows the new clusters to grow abnormally fast and they are "able to survive" in this region beyond onset, i.e. the point of maximum supersaturation. The average-growth model also produces larger clusters, hence the lower number of clusters at onset as seen in the droplet concentrations at the x = 14 cm location in Fig. 10.

The most probable size is 45Å, 30Å and 25Å from top to bottom which gives a substantial difference in most probable mass or number of atoms per cluster in the ratio of 5.8:1.7:1.

Comparison of Growth Theories to Experiment

A detailed comparison of the droplet growth laws presented above has been made for one of the experiments both in terms of mass condensed and light scattering. The comparison for mass condensed is shown in Fig. 11. The experimental points in 11A and B come from a solution to the gasdynamic equations (1)-(4) plus the static pressure data. In order to relate heat release to mass fraction condensed the usual relation $dq = Ldg$ is employed. For moist air expansions this is an excellent assumption, however in steam expansions droplet temperatures maybe as large as 30°C above the ambient vapor temperature [15]. However, for water with a latent heat in the neighborhood of 600 cal/g the error involved is about 5%. Thus the error in g from experiment is such that the actual g at any point can be as much as 5% higher than the values shown in the experimental values of Fig. 11. Frequently the temperature increase is less than 30°C, but in any event this is not a serious error.

A variety of growth laws are shown in Fig. 11A. The solid curves 1 to 6 (these numbers refer to the nucleation and growth conditions listed in Table I) are all computed with no correction to the classical nucleation rate, i.e. $C = 1$ in Eq. (5). The three solid curves shown only part way up are estimated by interpolation between existing computer solutions. The three dotted curves 7-9 are for the nucleation rate decreased by the amount $C = \xi = 0.04$. This decrease in nucleation rate can be interpreted as the approximate non-isothermal correction [46,21] or, in the case of curves 7 and 9, as the factor ξ for the flux rate of clusters past the critical size.

In this particular example the theoretical range in onsets at $g = 0.001$ vary over $\Delta x \tilde{=} 1$ cm for the constant nucleation rate cases 1-6 and a span of $\Delta x = 0.5$ cm for the $C = \xi = 0.04$ cases 7-9 and a total span of $\Delta x = 1.5$ cm. This results in a span in Δp and ΔT for the three ranges above of 16, 13, and

22 torr; and 11, 11, and 18°C respectively. Of course this represents a considerable variety of possible growth laws whereas careful consideration of the more probable range in their adjustable parameters such as α, ξ, etc., can reduce these uncertainties by perhaps half. Nevertheless a not insignificant range in theoretical onsets conditions prevail.

The effect on g of a range in nucleation rates for the above Experiment 252, using the same growth law, due to Gyarmathy [39], is shown in Fig. 11B. Thus is is seen that the span in Δx at onset for constant nucleation rate and a variety of growth models, curves 1-6 of Fig. 11A is equivalent to a variation in nucleation rates in Fig. 11B of $C = 10^{-2}$ to $C = 10^{2}$ or a span of 10^{4} in J.

Wegener and Pouring [25] found that in their moist air experiments, g = 0.0001 gm of condensate/gm of flow was consistent with onset, while in this work the mass fraction condensed at onset is near g = 0.001 gm/gm of flow. The reason the growth models affect the predicted onset is that most of the mass condensed at onset was found to be due to growth. For the cases presented in Fig. 11, the average-growth model of Hill, curve 7, resulted in 99% of the mass condensed at onset due to growth, and the radius-dependent models of Hill and Gyarmathy, curves 3 and 9, resulted in 92% and 76% respectively, while for moist air expansions the mass condensed at onset due to growth is a small fraction of g.

The light scattering data for Experiment 252 is shown in Fig. 12 as circles. The theoretical light scattering for this experiment is shown for 6 of the 9 nucleation and growth conditions of Table I. The data separates more-or-less into two groups, the solid curves 1, 3 and 4 using the classical nucleation rate, and the dashed curves 7-9 with $J = 0.04J_{cl}$. The three solid curves fit the shape of the data best although the Wu and Hill growth law, curves 1 and 4, have an upper limit value of $\xi = 1$ which is not physically reasonable. This leaves the two possibilities of using the Wu growth with a more realistic ξ

which will shift it closer to the data or the use of the Gyarmathy growth expression, curve 3. The relative value of scattered light intensities through the condensation zone have little error associated with them. However the value of I_o has considerable uncertainty in its value since the main laser beam intensity had to be reduced by a factor of 10^{10} or more using window reflections and neutral density filters in order to be detected on the same photomultiplier tube as used for the scattered light. This error could be as large as $\pm$ 50% in this work but could be reduced with very careful calibration procedures.

However it is interesting to note that if the Gyarmathy growth law, Number 3 of Table I and Figs. 11A and 12, is used with a small increase in nucleation rate (a factor of C = 4 to 10, an insignificant change in J) the g vs. x curve will fit the data very well. Carrying this shift over to the light scattering data will also provide an excellent fit if the data is shifted very slightly upward by a change in I_o much smaller than its error limits.

DROPLET AGGLOMERATION

The modification of the droplet size distribution with time (or distance along the nozzle) will proceed at some finite rate as droplets may collide with each other and stick together. Two mechanisms may be involved to effect this process, Brownian motion and relative motion due to vapor-particle drag in an accelerating flow. The latter mechanism is expected to be negligible due to the very small droplet sizes and the magnitude of accelerations encountered in the condensation zone [23]. The former mechanism can be tested using an agglomeration rate expression and a typical mean droplet radius. The agglomeration rate is estimated using two rate expressions. The first one considered here is due to Roberts [33] in which it is stated that the use of an average droplet radius would over-estimate the collision rate when working in the free-molecular regime. This collision rate obtained from kinetic theory for

uniform-sized particles is

$$\frac{dN}{dt} = -c \left[\frac{48kT}{\rho_c}\right]^{1/2} r^{-1/2} N^2 \quad . \tag{17}$$

The second version is from Brock and Hidy [47] and is given by the equation

$$\frac{N}{N_o} = \frac{1}{(1 + 6.8 \times 10^{-12} N_o^{5/6} c_o^{1/6} T^{1/2} ct)^{6/5}} \quad . \tag{18}$$

Both versions have been applied to the thermodynamic conditions of the condensation zone of Experiment 252. At onset the vapor concentration is the highest in the condensation zone at $c_o = 3.86 \times 10^{18}$ molecules/cm^3, $\bar{r} \tilde{=} 10^{-7}$ cm = 10Å, and t = 40μsec through the zone ($x \tilde{=}$ 11.5 to 14 cm). The results are presented in Table II. They all show a minor change in droplet concentration as is the case for moist air [48]. Even for the absolute upper bound the effect is only 7.4% on droplet concentration and 14.8% on the light scattering at x = 14 cm. It goes monotonically to 0% at onset. The more probable upper bound is that of Number 5 and 6 giving only a 0.4-1.8% maximum change in light scattering. Thus the frequently encountered case of droplet distributions in supersonic nozzles is one having small agglomeration rates. This feature is one that makes nozzles attractive for the study of droplet growth without having to deal with a very complicated stochastic agglomeration or cloud coalescence phenomena.

CONCLUSIONS

The thermodynamic results for this work have been summarized in Table III. The steam expansions were tested with four stages of increased filtering with no change in condensation onset characteristics thus ensuring the clustering process was a homogeneous one. A factor of 15 in laser power at 514.5 nm up to 1.5 watts was used to verify the theoretical expectation that the photon flux would not alter the nature of the phase change. The use of both static pressure and light scattering measurements proved to be complimentary for some operating conditions providing two tests instead of one for combinations of nucleation and growth laws. The light scattering proved to be more sensitive to changes in droplet size distributions than the static pressure. Also, if agglomeration had been a factor the light scattering would provide a sensitive measure of this process whereas there would be no change in static pressure. Moreover, it was found that the light scattering is a simpler and more positive test,for those expansions from lower pressure,than static pressure measurements.

The dual measurements were helpful in making comparisons to the theory since nucleation and growth are coupled even at onset. The computer solutions estimated from 75% to 99% of the mass condensed at onset being due to growth depending on the growth models employed. The full range of growth laws considered in the detailed comparison with Experiment 252 gave a span in onset pressure and temperature of Δp = 22 torr and ΔT = 18 ^{o}C. With insignificantly small adjustments the classical nucleation and Gyarmathy growth law provided an excellent match to both static pressure and light scattering. Finally, the use of supersonic nozzles for the study of droplet growth is especially advantageous since there is no significant agglomeration. Also, the use of carrier gas expansions, such as moist air, etc. where the condensable species

is a small mole fraction in the expansion, is ideal for the study of homogeneous nucleation. For this case the condensed mass at onset is nearly all due to nucleation and thus the growth law is not coupled to the nucleation rate.

ACKNOWLEDGEMENTS

The authors would like to thank the Power Branch of the Office of Naval Research and the Engineering Division of the National Science Foundation for partial financial support. We also thank Mr. R. Klaub and his machine shop for their continuous support for the experimental apparatus and acknowledge the use of the computer facilities of the Southwest Research Institute for some of the data analysis and theoretical solutions.

REFERENCES

1. Stodola, A., Steam and Gas Turbines, McGraw-Hill Book Company, Inc., New York, 1927.

2. Binnie, A. M., and M. W. Woods, "The Pressure Distribution in a Convergent-Divergent Steam Nozzle," Proc. Inst. Mech. Eng., Vol. 138, 1938, p. 229.

3. Binnie, A. M., and J. R. Green, Proc. Roy. Soc. (London), Vol. 181A, 1942, p. 134.

4. Oswatitsch, K., "Die Nebelbildung in Windkanälen und ihr Einfluss auf Modellversuche," Jahrb. d. deufsch. Luftfahrtforshung, Vol. 1, 1941, pp. 692-703.

5. Oswatitsch, K., "Kondensationserscheinungen in Überschalldüsen," Zamm, Vol. 22, 1942, p. 1.

6. Oswatitsch, K., "Kondensationsstösse in Lavaldüsen," Z. Ver. deutsch. Ing., Vol. 86, 1942, p. 402.

7. Stever, H. G., and K. C. Rathbun, "Theoretical and Experimental Investigation of Condensation of Air in Hypersonic Wind Tunnels," NACA TN 2359, 1951.

8. Head, R. M., "Investigation of Spontaneous Condensation Phenomena," Ph.D. Thesis, California Institute of Technology, Pasadena, CA, 1949.

9. Buhler, R., "Condensation of Air Components in Hypersonic Wind Tunnels," Ph.D. Thesis, California Institute of Technology, Pasadena, CA, 1949.

10. Arthur, P. D., "Effects of Impurities on the Supersaturation of Nitrogen in a Hypersonic Wind Tunnel," Ph.D. Thesis, California Institute of Technology, Pasadena, CA, 1952.

11. Willmarth, W. W., and H. T. Nagamatsu, "The Condensation of Nitrogen in a Hypersonic Nozzle," J. Appl. Phys., Vol. 23, 1952, pp. 1089-1095.

12. Winkler, E. M., "Condensation Study by Absorption or Scattering of Light," Physical Measurements in Gas Dynamics and Combustion, (Princeton University Press, Princeton, NJ), Vol. IX, 1954, pp. 289-304.

13. Gyarmathy, G., "Kondensationsstoss-Diagramme für Wasserdampfströmungen," Forsch. Ing. Wes., Vol. 29, 1963, p. 105.

14. Gyarmathy, G., and H. Meyer, "Spontane Kondensation (VDI Forsch.-Heft 508)," Dusseldorf, VDI Verlag, 1965.

15. Hill, P. G., "Condensation of Water Vapor During Supersonic Expansion in Nozzles," J. Fluid Mech., Vol. 25, 1966, p. 593.

16. Jaeger, H. L., E. J. Willson, P. G. Hill, and K. C. Russell, "Nucleation of Supersaturated Vapors in Nozzles, I. H_2O and NH_3," J. Chem. Phys., Vol. 51, No. 12, December 13, 1969, pp. 5380-5388.

17. Dawson, D. B., E. J. Willson, and P. G. Hill, "Nucleation of Supersaturated Vapors in Nozzles. II. C_6H_6, $CHCl_3$, CCl_3F and C_2H_5OH," J. Chem. Phys., Vol. 51, 1969, pp. 5389-5397.

18. Barschdorff, D., "Dichtemessungen in Wasserdampfströmungen mit einem Differentialinterferometer," Photographie und Film in Industrie und Technik III, Darmstadt-Wien, Verlag Dr. Othmar Helwich, 1971, p. 155.

19. Barschdorff, D., "Verlauf der Zustandsgrössen und gasdynamische Zusammenhänge dei der spontanen Kondensation reinen Wasserdampfes in Lavaldüsen," Forsch. Ing. Wes., Vol. 37, 1971, p. 146.

20. Barschdorff, D., and G. A. Fillipov, "Analysis of Certain Special Operating Modes of Laval Nozzles with Local Heat Supply," Energetika i Transport, Vol. 3, 1970, p. 94. Also Heat Transfer (Soviet Research, Vol. 2, 1970, p. 76.

21. Barschdorff, D., W. J. Dunning, P. P. Wegener, and B. J. C. Wu, "Homogeneous Nucleation in Steam Nozzle Condensation," Nature Physical Science, Vol. 140, 1972, p. 167.

22. Wegener, P. P., "Water Vapor Condensation Process in Supersonic Nozzles," J. Appl. Phys., Vol. 25, 1954, p. 1485.

23. Wegener, P. P., and L. M. Mack, "Condensation in Supersonic and Hypersonic Wind Tunnels," Adv. Appl. Mech., Vol. 5, New York, Academic Press, 1958, p. 307.

24. Wegener, P. P., "Condensation Phenomena in Nozzles," Progress Astron. Aero., Vol. 15, New York, Academic Press, 1964, p. 701.

25. Wegener, P. P., and A. A. Pouring, "Experiments on Condensation of Water Vapor by Homogeneous Nucleation in Nozzles," Phys. Fluids, Vol. 7, 1964, p. 352.

26. Stein, G. D., and P. P. Wegener, "Experiments on the Number of Particles Formed by Homogeneous Nucleation in the Vapor Phase," J. Chem. Phys., Vol. 46, 1967, p. 3685.

27. Wegener, P. P., "Gasdynamics of Expansion Flows with Condensation, and Homogeneous Nucleation of Water Vapor," Nonequilibrium Flows (P. P. Wegener, ed.), Vol. 1, Part 1, New York, Marcel Dekker, 1969, p. 163.

28. Wegener, P. P., and J.-Y. Parlange, "Condensation by Homogeneous Nucleation in the Vapor Phase, Naturwissenschaften, Vol. 57, 1970, p. 525.

29. Wegener, P. P., J. A. Clumpner, and B. J. C. Wu, "Homogeneous Nucleation and Growth of Ethanol Drops in Supersonic Flow," Phys. Fluids, Vol. 15, 1972, p. 1869.

30. Wegener, P. P., "Nonequilibrium Flow with Condensation," Acta Mechanica Vol. 21, 1975, pp. 65-91.

31. Stein, G. D., and C. A. Moses, "Rayleigh Scattering Experiments on the Formation and Growth of Water Clusters Nucleated from the Vapor Phase," J. Coll. and Interface Sci., Vol. 39, 1972, pp. 504-512.

32. Stein, G. D., "Angular and Wavelength Dependence of the Light Scattered from a Cloud of Particles Formed by Homogeneous Nucleation," J. Chem. Phys., Vol. 51, 1969, p. 938.

33. Roberts, R., "A Light Scattering Investigation of Droplet Growth in Nozzle Condensation," Gas Turbine Laboratory Report No. 97, Massachusetts I ..titute of Technology, Cambridge, MA., February, 1967.

34. Pound, G. M., "Selected Values of Critical Supersaturation for Nucleation of Liquids from the Vapor," J. Phys. Chem. Ref. Data, Vol. 1, No. 1, 1972, p. 119.

35. Volmer, M., Z. Phys. Chem., Vol. 25, 1929, p. 555.

36. Volmer, M., Kinetik der Phasenbildung, Steinkopf, Dresden and Leipzig, 1939, p. 148.

37. Katz, J. L., private communication.

38. Lewis, J. W. L., W. D. Williams, and H. M. Powell, Rarefied Gas Dynamics, Vol. II (M. Becker and M. Fiebig, eds.) DFVLR Press, Porz-Wahn, Germany, 1974, pp. F7-1 to F7-8.

39. Gyarmathy, Georg, "Zur Wachstumsgeschwindigkeit kleiner Flussigkeitstropfen in einer ubersattigten Atmosphare," Zeitschrift Fur Angewandt Mathematik und Physik (ZAMP), Vol. 14, No. 3, 1963, p. 280.

40. Wachman, H. Y., "The Thermal Accommodation Coefficient: A Critical Survey," ARS Journal, January 1962, p. 2.

41. Alty, T., "The Exchange of Energy Between a Gas and a Solid or Liquid Surface," Science Progress, Vol. XXXI, 1936-37, p. 436.

42. Alty, T., and C. A. Mackay, "The Accommodation Coefficient and the Evaporation Coefficient of Water," Proceedings of the Royal Society, Vol. 149, 1935, p. 104.

43. Kramers, H., and S. Stemerding, "The Sublimation of Ice in a Vacuum," Appl. Sci. Res., (Hague), Vol. A3, p. 73.

44. Campbell, B. A., and F. Bakhtar, "Condensation Phenomena in High Speed Flow of Steam," Proc. Instn. Mech. Engrs., Vol. 185, No. 25/71, 1970-71, p. 395.

45. Wu, B. J. C., "Computer Programs for Calculating Condensation Rate in Steady, Adiabatic Expansions in Supersonic Nozzles," Report #26 on ONR Contract N00014-67-A-0097-0012, Yale University, 1974, 111 pages.

46. Feder, J., K. C. Russell, J. Lothe, and G. M. Pound, "Homogeneous Nucleation and Growth of Droplets in Vapors," Adv. Phys. (Suppl. Phil. Mag.) Vol. 15, 1966, pp. 111-178.

47. Brock, J. R., and G. M. Hidy, "Collision-Rate Theory and the Coagulation of Free-Molecule Aerosols," J. Appl. Phys., Vol. 36, 1965, pp. 1857-1862.

48. Wegener, P. P., and G. D. Stein, "Light Scattering Experiments and Theory of Homogeneous Nucleation in Condensing Supersonic Flow," Twelfth Symposium (International) on Combustion, 1969, pp. 1183-1191.

TABLE I

SUMMARY OF NUCLEATION AND GROWTH LAW COMBINATIONS

Number	Reference and Description	Mass Accommodation Coefficient ξ	Nucleation Rate Factor C ($J = CJ_{classical}$)
1	Wu [45]	N.A.	1
2	Hill, surface-averaged radius [15]	1.0	1
3	Gyarmathy, radius-dependent [39]	N.A.	1
4	Hill, radius-dependent [15]	1.0	1
5	Hill, surface-averaged [15]	0.04	1
6	Hill, radius-dependent [15]	0.04	1
7	Hill, surface-averaged radius [15]	0.04	0.04
8	Gyarmathy, radius-dependent [39]	N.A.	0.04
9	Hill, radius-dependent [15]	0.04	0.04

TABLE II

CALCULATIONS OF DROPLET AGGLOMERATION IN THE CONDENSATION ZONE

Number	Equation	Initial Concentration N_o cm^{-3}	Sticking Coefficient c	Concentration Ratio N/N_o	Fractional Concentration Change $\Delta N/N_o$	Fractional Light Scattering Change $\Delta(I/I_o)$ percent
1	17	10^{12}	1.0	0.980	0.020	4.0%
2	18	10^{12}	1.0	0.926	0.074	14.8%
3	17	10^{12}	0.1	0.998	0.0020	0.4%
4	18	10^{12}	0.1	0.992	0.008	1.6%
5	17	3×10^{11}	0.3	0.998	0.0018	0.4%
6	18	3×10^{11}	0.3	0.991	0.009	1.8%
7	17	10^{11}	1.0	0.998	0.0020	0.4%
8	18	10^{11}	1.0	0.988	0.012	2.4%

TABLE III

SUMMARY OF EXPERIMENTS

Exp. No.	Type *	Starting Conditions		Onset Conditions					
		P_o (torr)	T_o (°K)	x(cm)	A/A*	P(torr)	T(°K)	S	r*(Å)
178	P	202.5	377.2	12.78	1.2797	48.6	268.7	14.7	4.6
183	P	146.9	365.2	12.50	1.2496	37.0	262.8	17.7	4.4
187	P	227.8	373.6	12.22	1.2191	60.8	273.0	13.4	4.6
191	P	133.6	369.2	13.26	1.3365	29.3	257.4	21.7	4.2
192	P	414.4	375.2	10.7	1.0906	146.5	292.6	8.7	5.0
193	P	322.7	366.0	10.74	1.0906	114.4	285.9	10.3	4.8
203	P&L	268.4	368.3	11.42	1.1428	84.3	280.7	10.8	4.8
203	P&L	206.2	367.9	11.90	1.1864	58.6	272.6	13.3	4.7
210	P&L	163.2	368.0	12.26	1.2234	43.2	268.2	13.6	4.7
214	P&L	192.3	368.2	12.18	1.2148	51.7	269.3	15.0	4.5
218	P&L	198.9	367.7	12.14	1.2106	53.8	269.2	15.8	4.4
220	P&L	179.9	366.9	12.18	1.2148	48.3	268.2	15.3	4.5
222	P&L	168.2	366.7	12.50	1.2496	42.6	264.9	17.3	4.4
226	L	310.7	380.0	12.06		87.9	278.6		
227	L	310.7	377.6	11.79		92.3	280.3		
228	L	310.7	375.6	11.52		97.2	282.6		
229	L	310.7	371.6	11.30		101.3	283.0		
230	L	310.7	370.9	11.05		105.9	285.0		
231	L	310.7	368.9	10.90		108.7	285.4		
233	L	262.2	365.7	11.10		88.6	280.0		
234	L	262.2	371.0	11.49		82.6	279.5		
235	L	262.2	374.5	11.79		77.9	278.1		
236	L	262.2	379.1	12.20		72.2	276.1		
237	L	262.2	382.8	12.60		66.9	273.5		
238	L	202.1	367.6	11.94		58.4	271.1		
239	L	202.1	367.2	11.92		58.6	271.2		
240	L	202.1	360.8	12.16		56.0	270.5		
241	L	202.1	374.4	12.43		53.2	269.7		
242	L	202.1	374.9	12.48		52.7	269.4		
243	L	202.1	379.4	12.81		49.7	268.4		
244	L	202.1	383.5	13.18		46.5	267.1		
245	L	146.2	365.1	12.47		38.2	261.0		
246	L	146.2	371.6	13.19		33.6	258.8		
247	L	146.2	375.6	13.49		31.8	257.8		
248	L	146.2	381.9	14.1		28.8	255.7		
249	L	146.2	382.3	14.1		28.8	255.9		
250	L	146.2	383.9	14.31		27.9	255.1		
251	L	146.2	377.1	13.82		30.1	255.1		
252	P&L	300.4	374.3	11.50	1.1496	92.2	282.7	10.3	4.9
254	P&L	394.0	372.8	10.70	1.0878	140.7	291.8	8.7	5.0
257	P&L	507.5	376.7	10.50	1.0746	188.3	297.6	8.2	5.0
258	P&L	402.0	372.8	10.58	1.0797	147.2	293.5	8.2	5.1
287	L	106.8	375.0	14.1		≈21.1#	≈251		
288	L	94.1	372.6	15.1		≈16.5#	≈241		
289	L	94.1	372.3	15.3		≈16.1#	≈240		
290	L	84.7	371.6	16.4		≈13.6#	≈235		
291	L	76.9	367.4	15.7		≈12.8#	≈235		

*P = pressure measurements; L = light-scattering measurements
#Nozzle was not "calibrated" this far downstream; see Figure 6 for error bars.

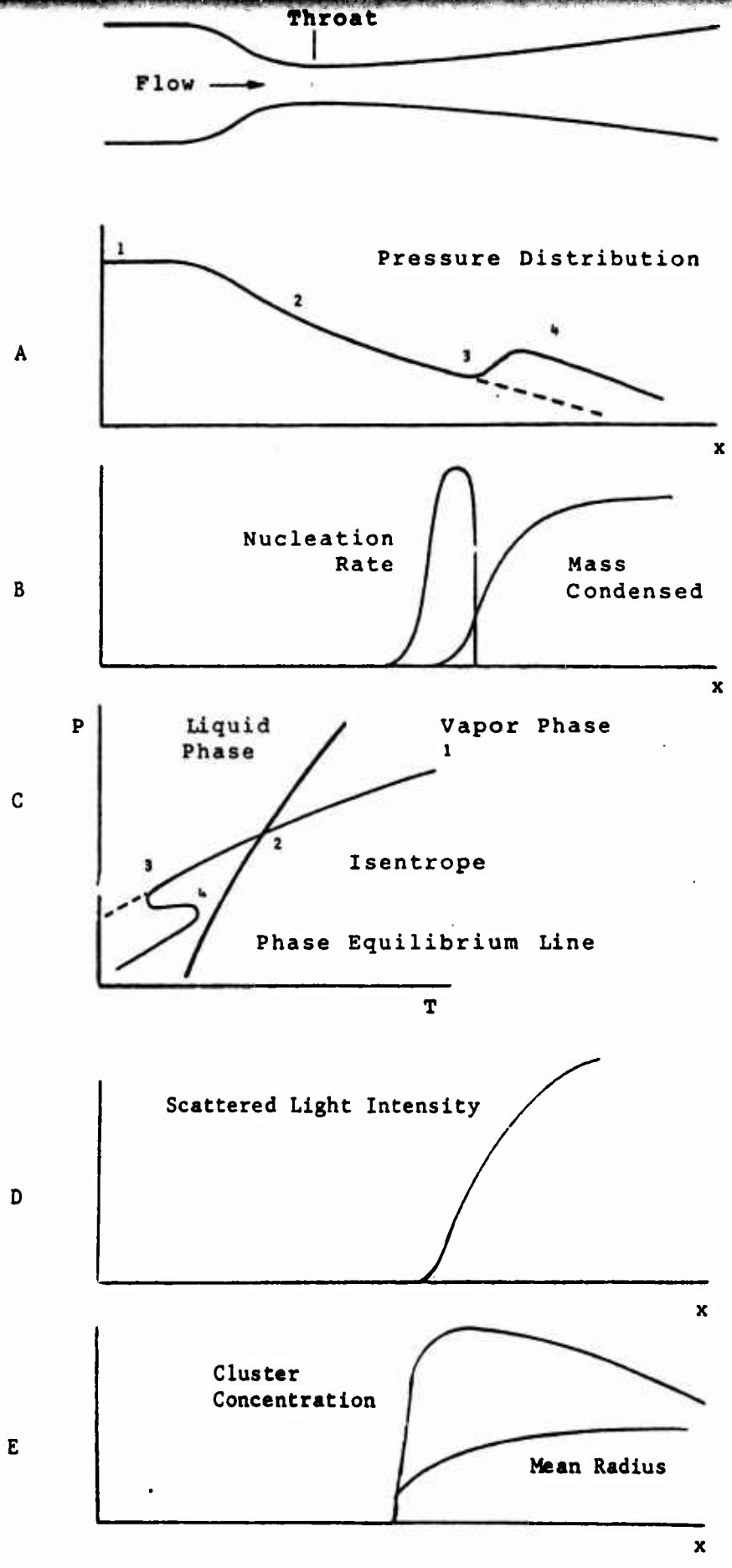

Figure 1. The dynamics of condensation is illustrated above with pressure and light scattering in A and D being the measured quantities and the remainder being derived quantities.

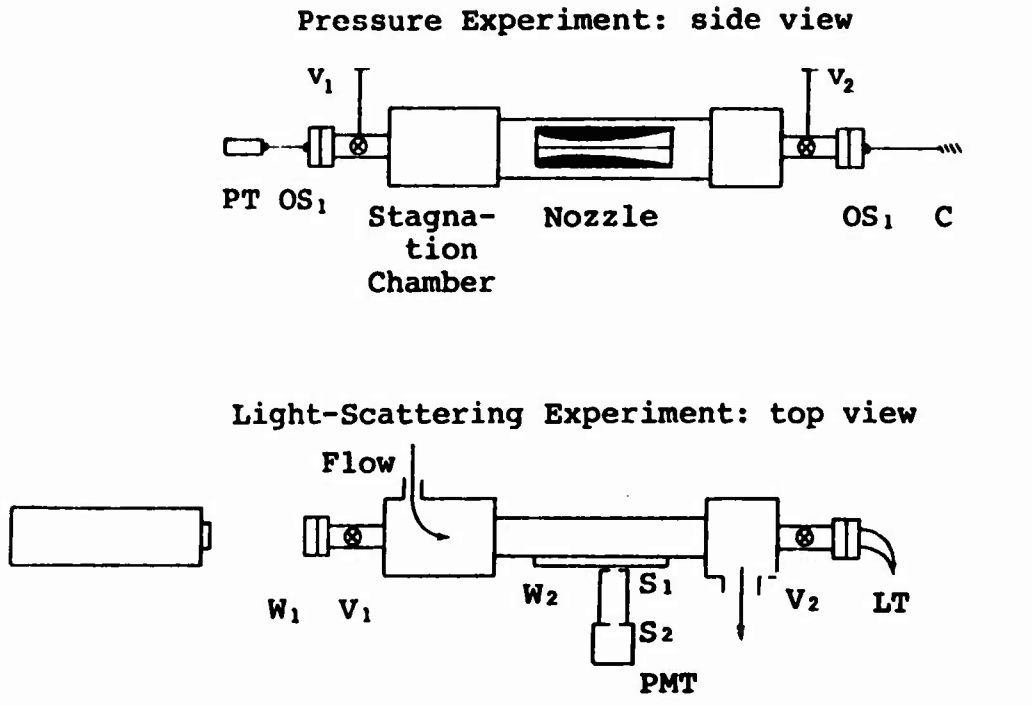

Figure 2. The schematic arrangement for the experiments is shown with the static pressure probe installed in the side view and the light scattering installed in the top view.

Nozzle Position	Effective Area Ratio
6.0	1.06598
6.5	1.03675
7.0	1.01695
7.5	1.00505
8.0	1.00018
8.5	1.00192
9.0	1.01024
9.5	1.02499
10.0	1.04699
10.5	1.07459
11.0	1.10945
11.5	1.14962
12.0	1.19625
12.5	1.24956
13.0	1.30431
13.5	1.36713
14.0	1.42761

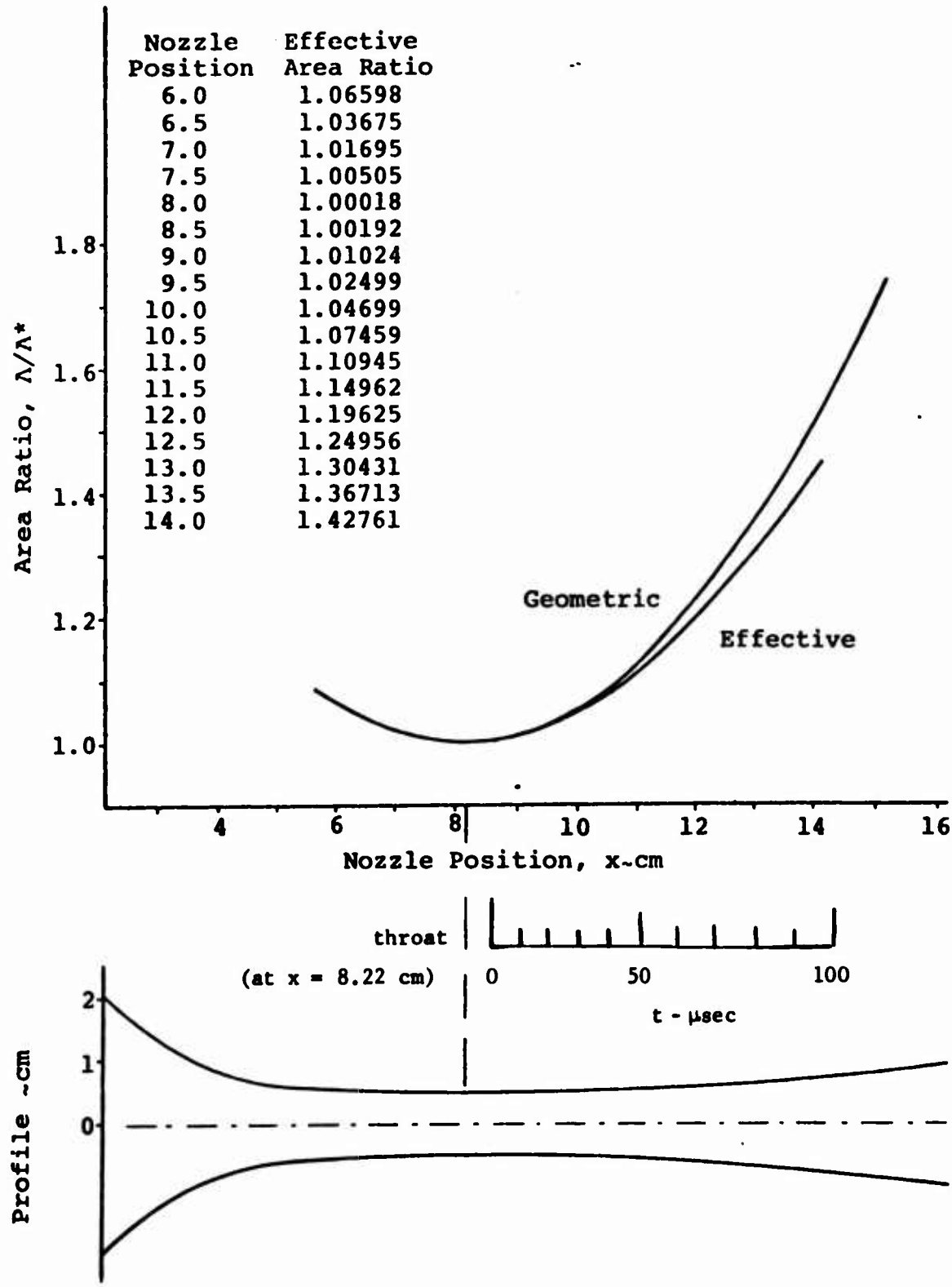

Figure 3. The actual nozzle geometry is shown above along with the area ratio plotted for the nozzle geometry and corrected for boundary layer growth. A typical time scale for motion with the flow is included.

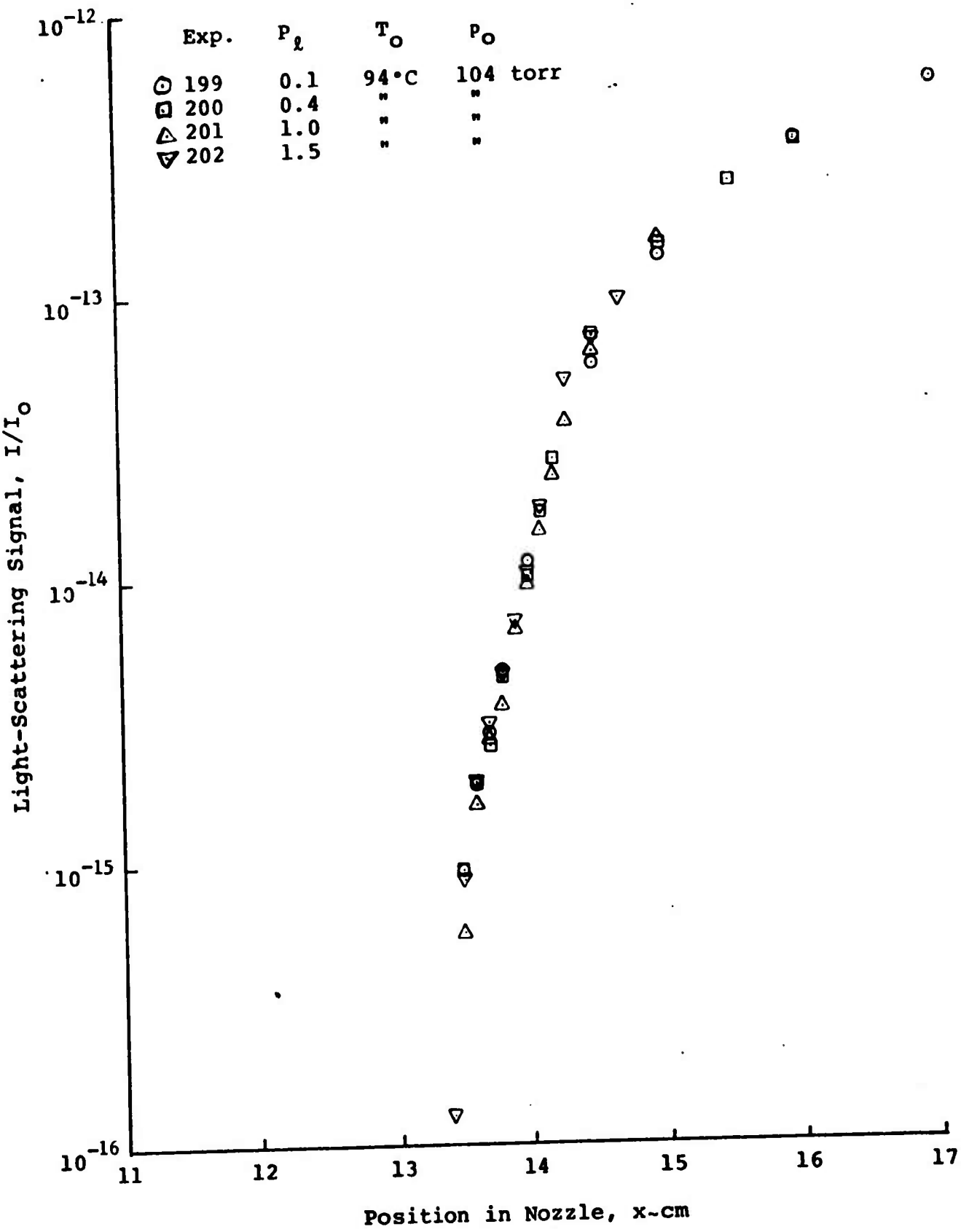

Figure 4. A linearity test of the light-scattering system shows that there is no effect on the nucleation and growth process for a range of 15:1 in laser power.

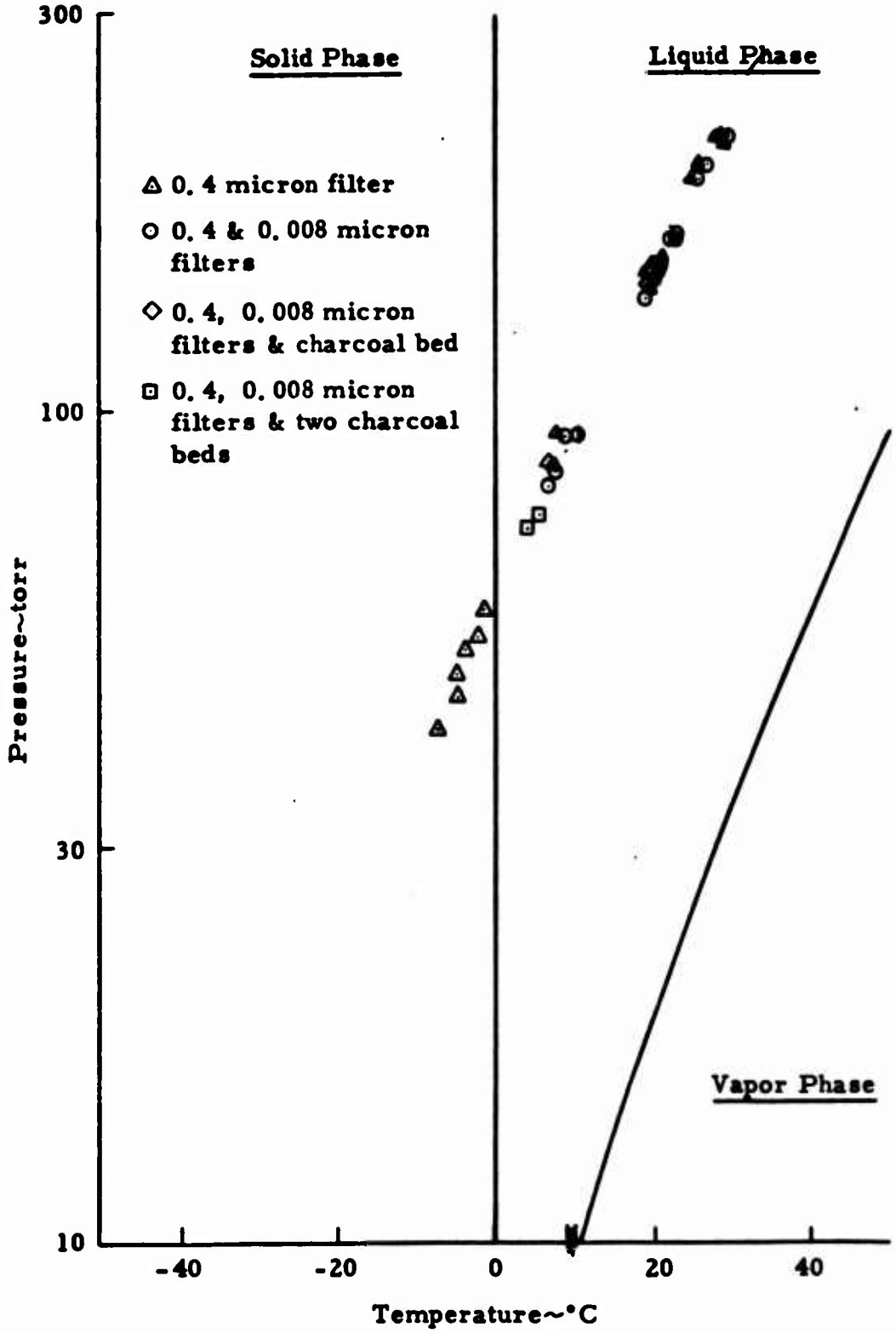

Figure 5. The locus of onset for experiments with different filters shows that there is no change in onsets of condensation thus eliminating heterogeneous nucleation as a competitive rate process with the homogeneous phase change.

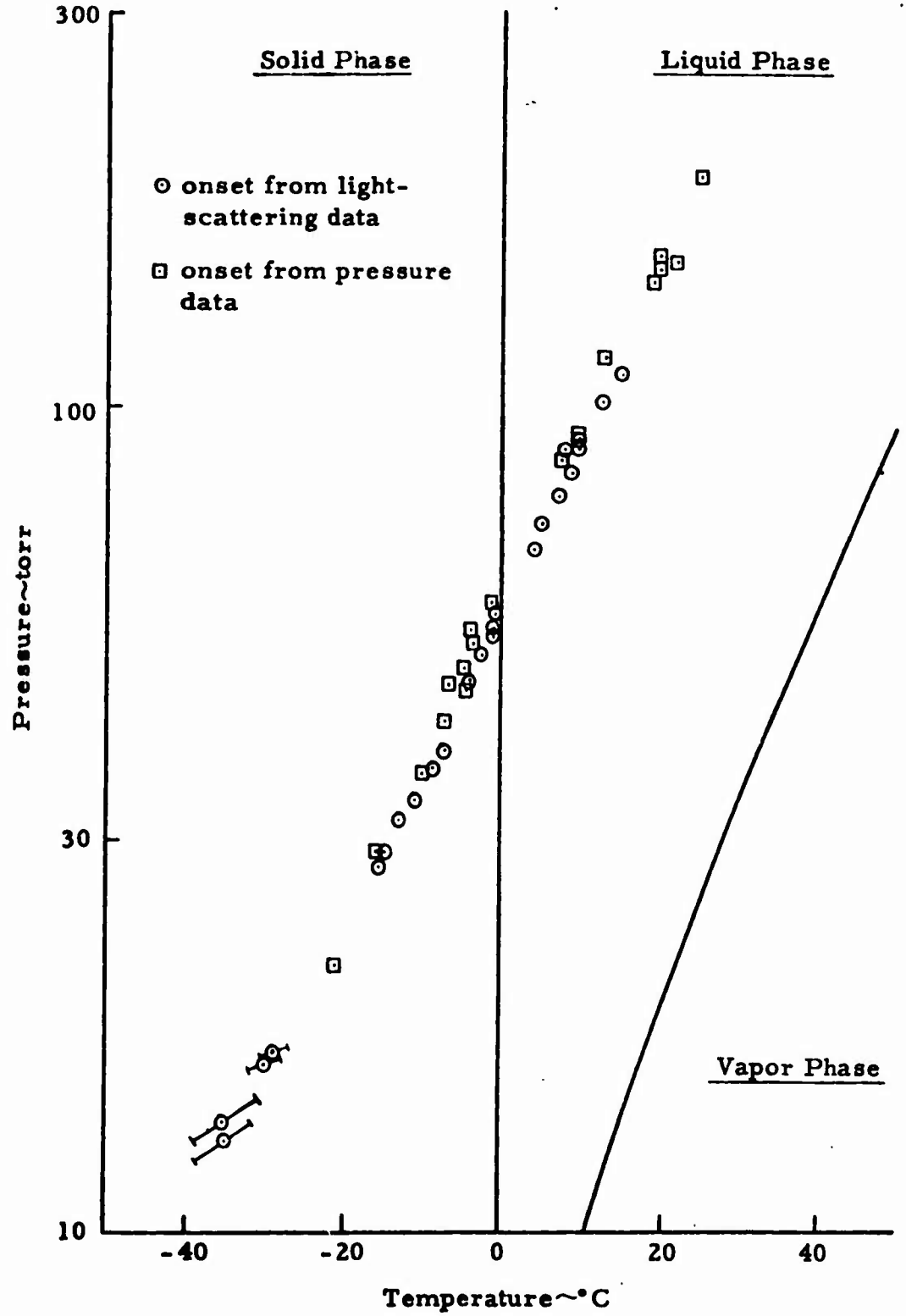

Figure 6. The location of onset for this work determined from static pressure measurements and light scattering shows that they provide effectively the same criteria. There appears to be a slight difference, with the light scattering predicting the onset a little closer to the vapor-liquid equilibrium line.

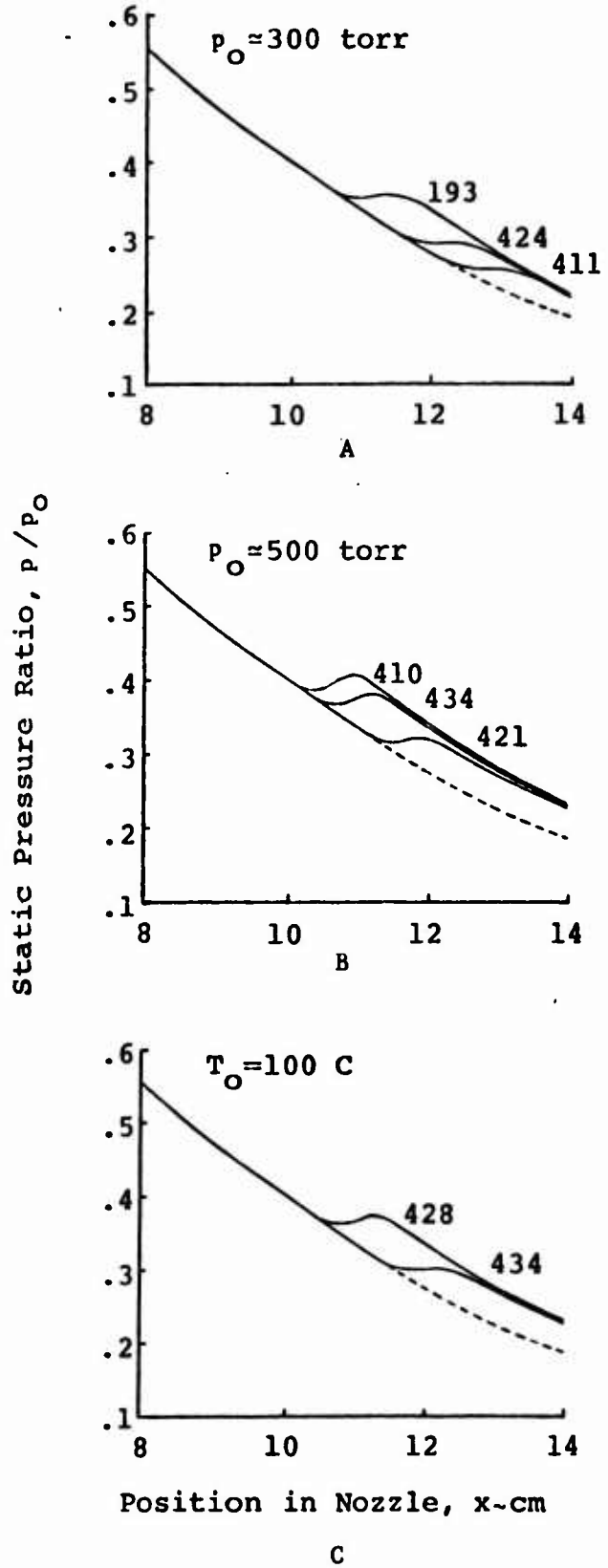

Exp.	p_o(torr)	T_o(°C)
193	322.7	93
424	314.3	103
411	317.1	112

Exp.	p_o(torr)	T_o(°C)
410	530.5	104
417	525.2	106
421	501.1	112

Exp.	p_o(torr)	T_o(°C)
428	410.3	100
434	310.2	100

Figure 7. A comparison of pressure distributions for various flow conditions is shown with pressure held nearly constant in A and B, and temperature held constant in C.

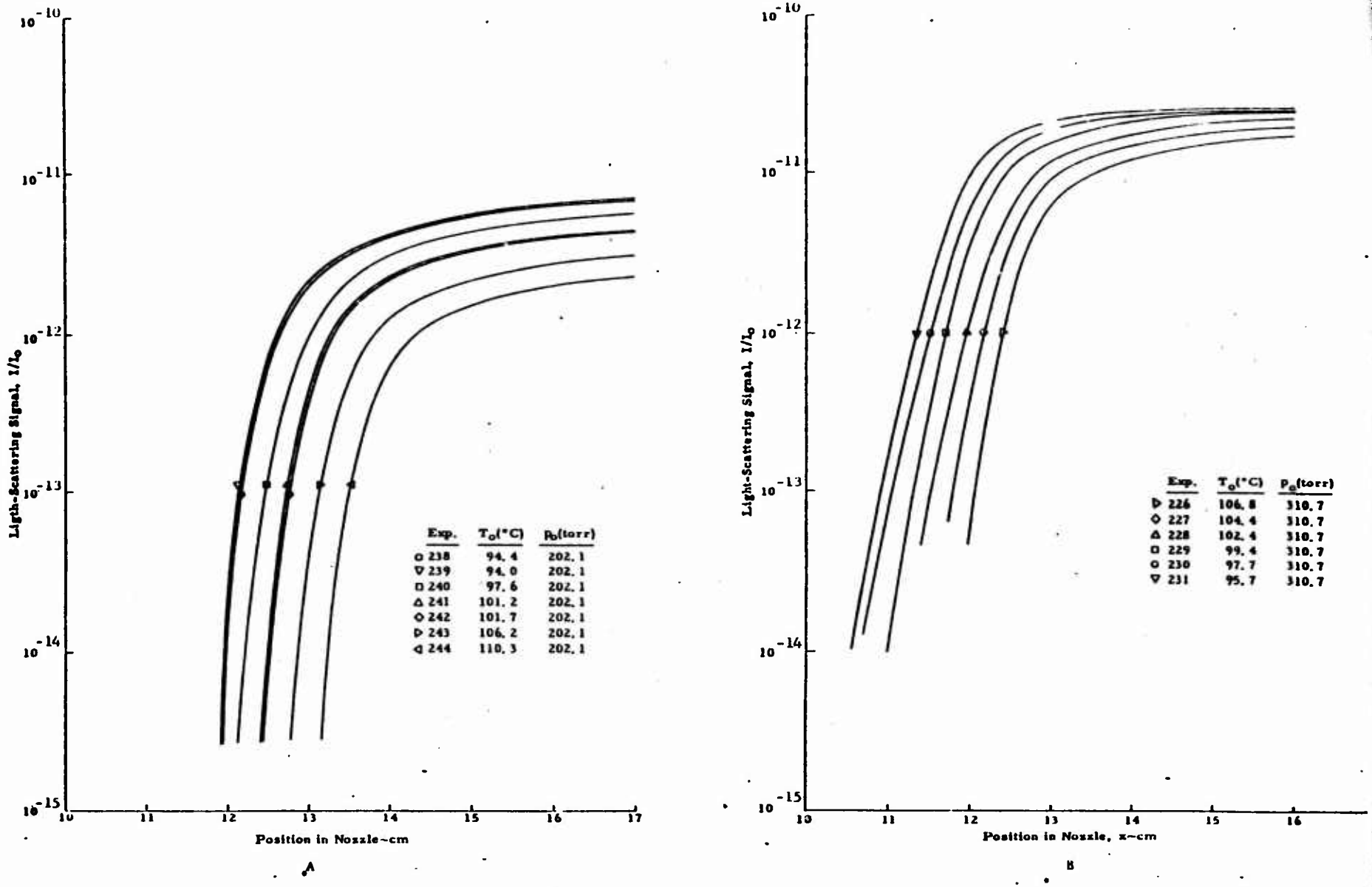

Figure 8. The variation of light scattering through the condensation zone is plotted for pressure held constant in A at 202.1 torr and at 310.7 torr in B.

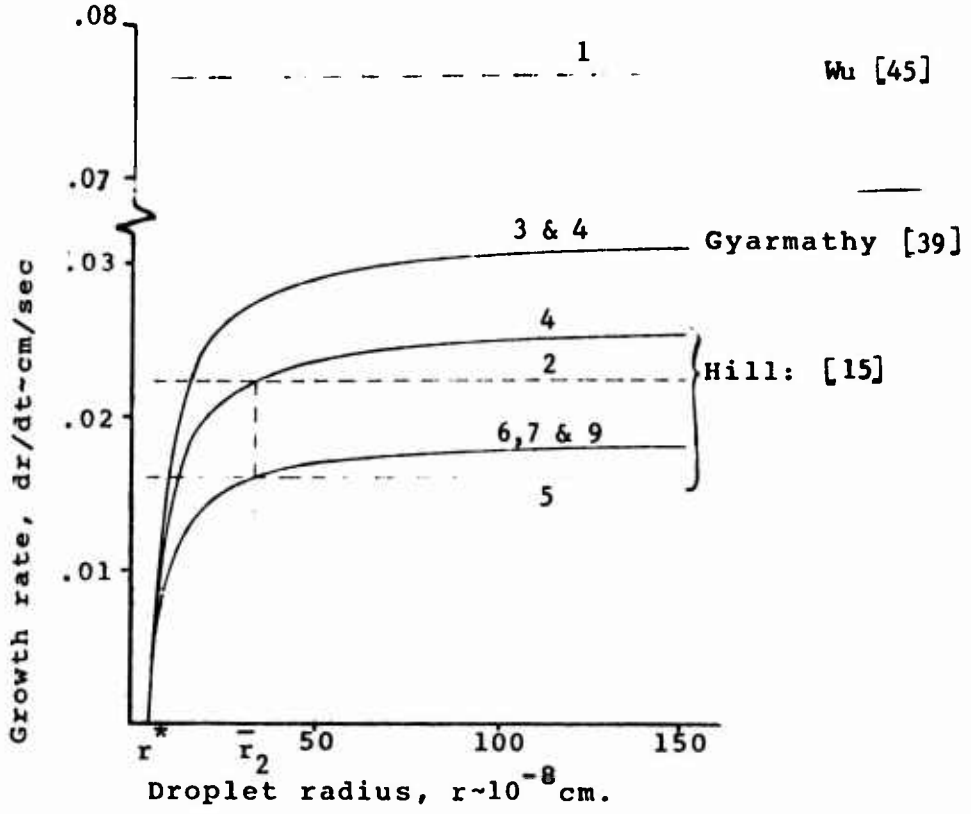

Figure 9. A comparison of droplet growth models is shown with the numbers corresponding to the conditions summarized in Table I.

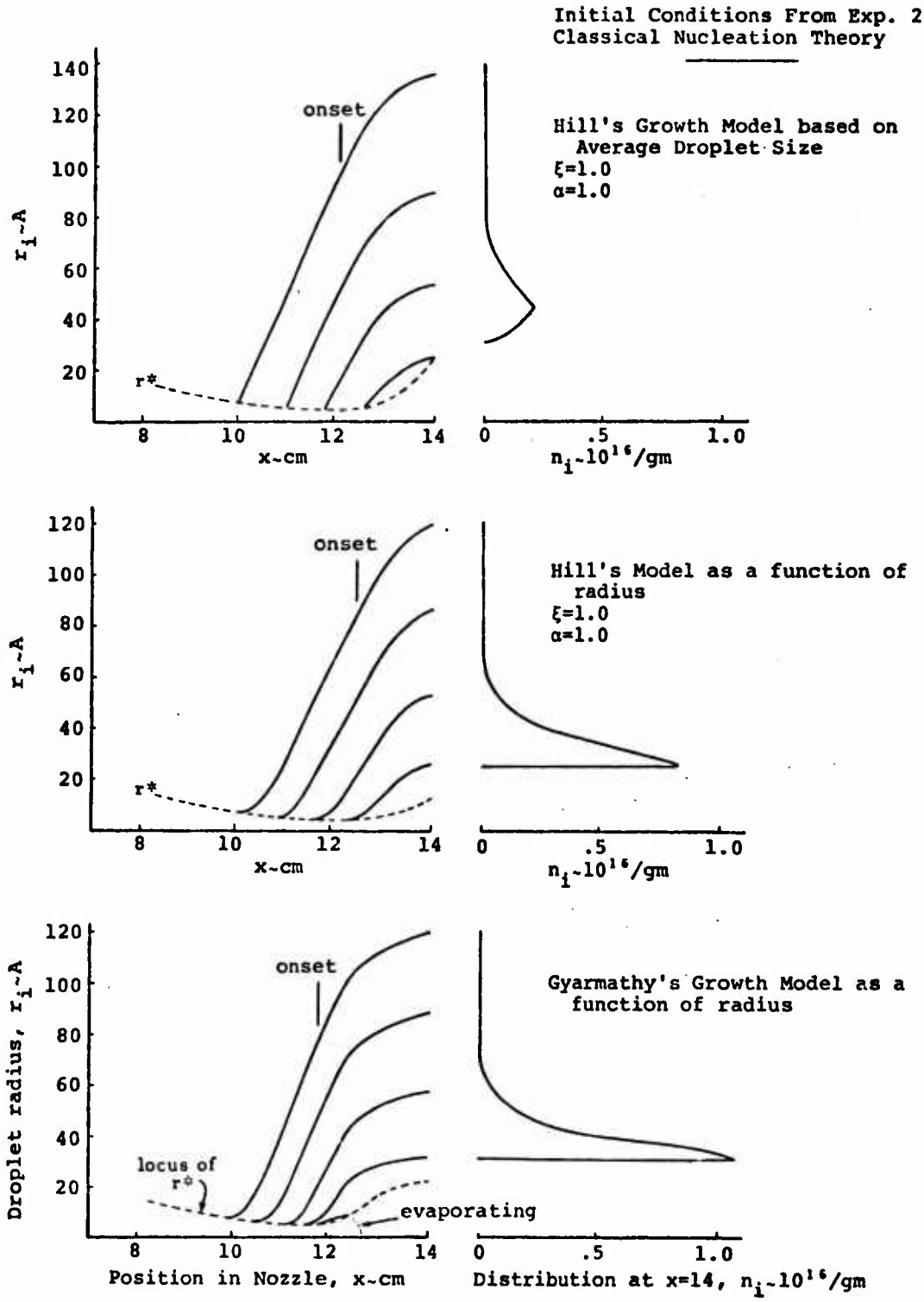

Figure 10. Predicted distribution and growth of droplets is documented for the growth models 2, 4, and 3 of Table I from top to bottom.

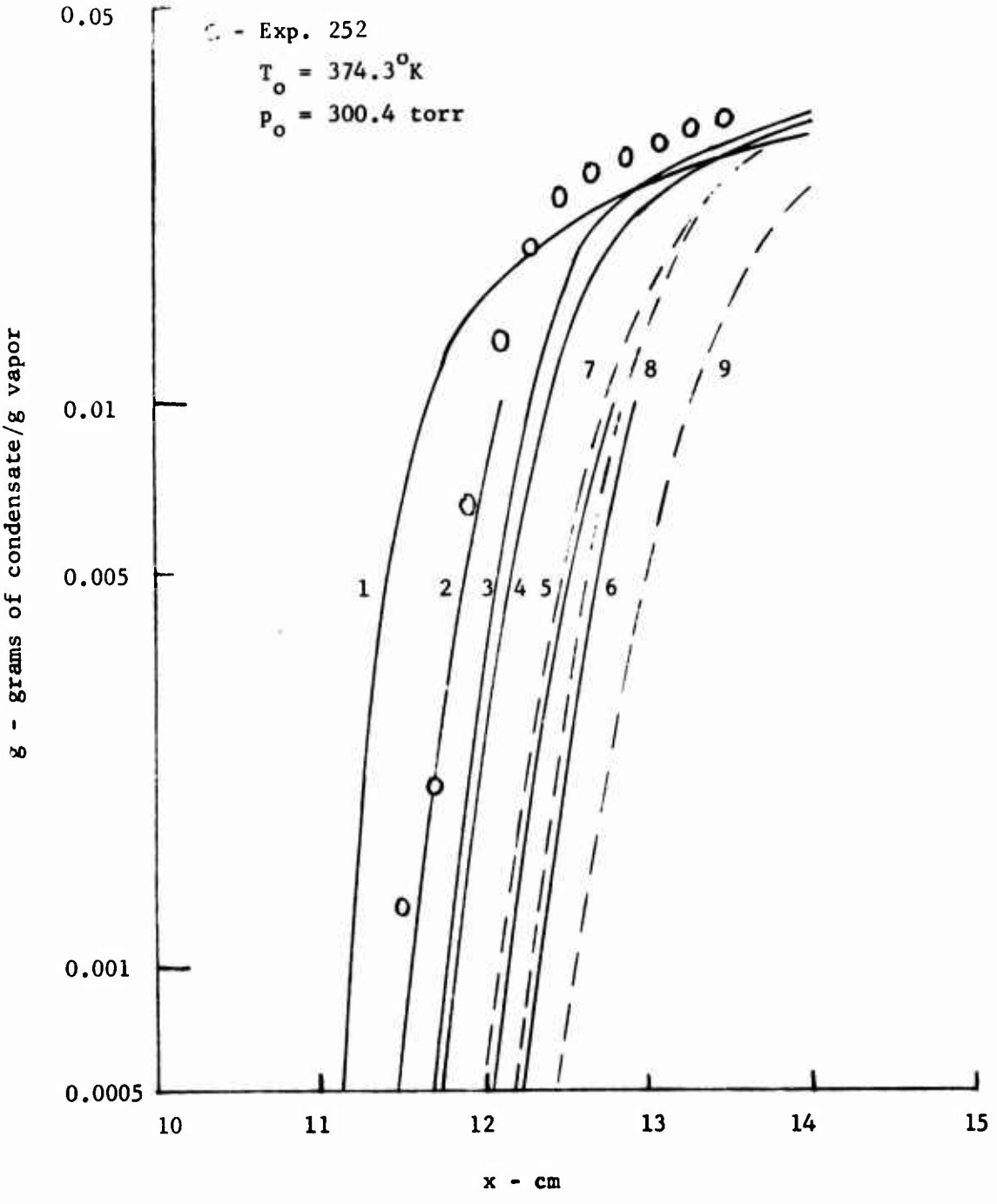

Figure 11A. The mass fraction condensed is plotted as circles from Exp. 252 with the first 6 growth laws using the classical nucleation rate, C = 1 in Eq. (5), while the last three use the correction C = ξ = 0.04. The curve numbers conform to those in Table I.

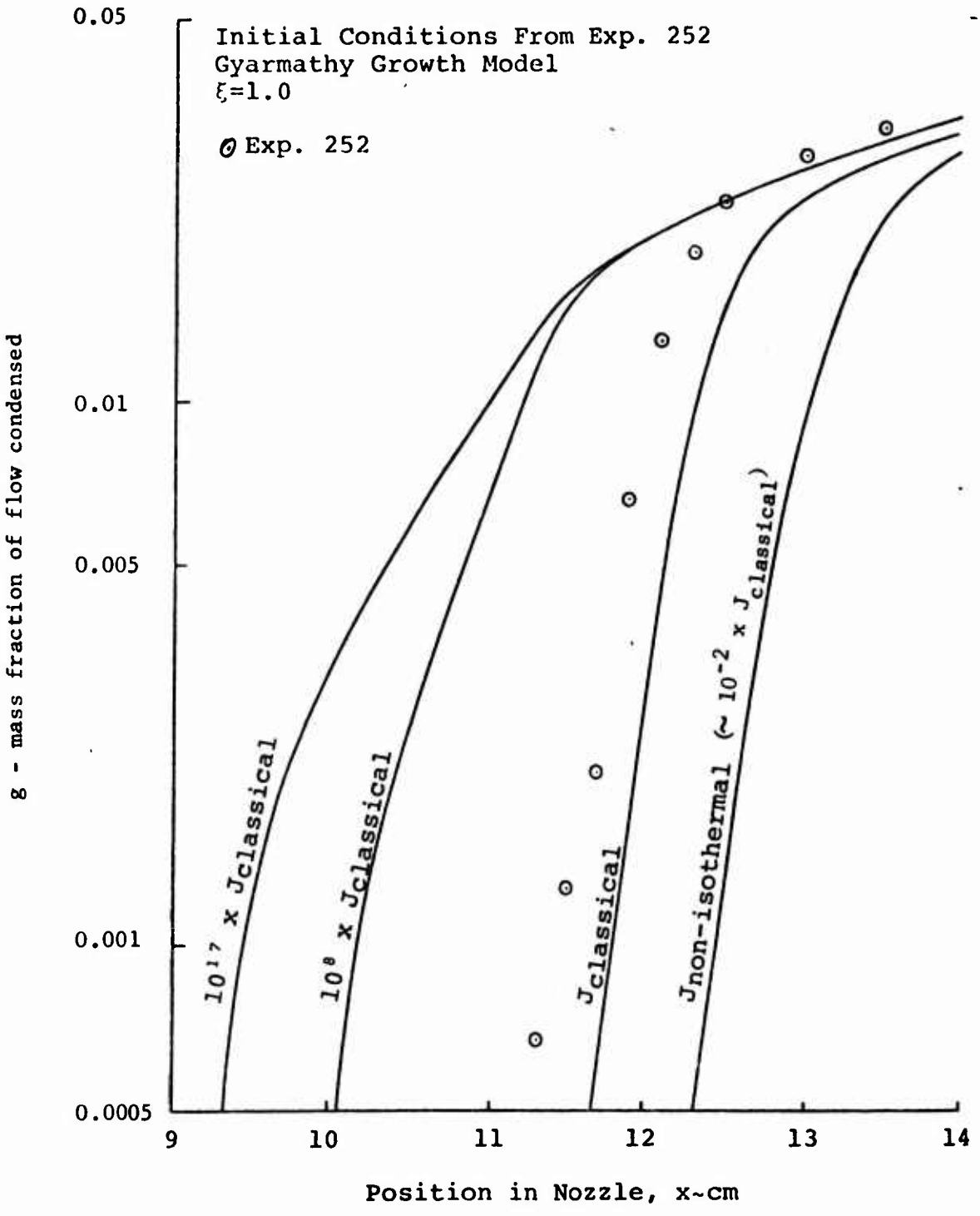

Figure 11B. The effect of different nucleation rates on the predicted condensed mass fraction is compared with the experimental values obtained from the static pressure measurements.

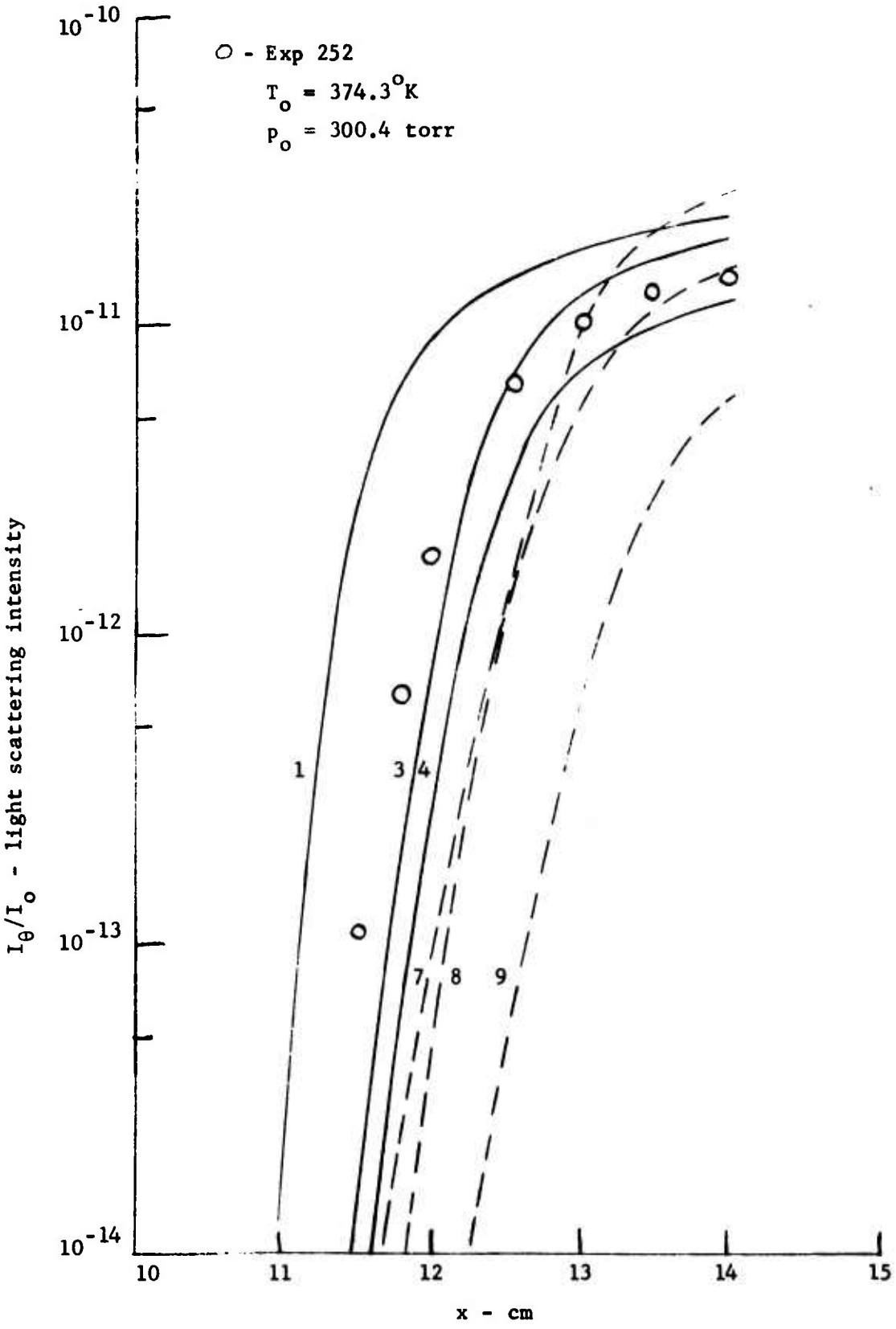

Figure 12. The light scattering at $\theta = 90^{\circ}$ is shown as circles for Exp. 252 with C = 1 in Eq. (5) for curves 1, 3, and 4, and C = ξ = 0.04 in 7, 8, and 9. (See Table I for additional information on the growth laws used.)